Materials Research Proceedings 41 (2024) 1106-1114 https://doi.org/10.21741/9781644903131-122

Tension-compression asymmetry of ferritic stainless steel sheet

Sekiya Koki[1,a], Higashii Hyuga[1,b] , Taoka Akira[2,c] and Kuwabara Toshihiko[3,d*]

[1]Department of Mechanical Systems Engineering, Graduate School of Engineering, Tokyo University of Agriculture and Technology, 2-24-16 Naka-cho, Koganei-shi, Tokyo 184-8588, Japan

[2]Raw Material Production Engineering Development Section, AISIN Co., 2-1 Asahi-cho, Kariya-shi, Aichi 448-8650, Japan

[3] Division of Advanced Mechanical Systems Engineering, Institute of Engineering, Tokyo University of Agriculture and Technology, 2-24-16 Naka-cho, Koganei-shi, Tokyo 184-8588, Japan

[a]sekiya@st.go.tuat.ac.jp, [b]s209914v@st.go.tuat.ac.jp, [c]a_taoka@koki.aisin.co.jp, [d]kuwabara@cc.tuat.ac.jp

Keywords: In-Plane Compression, Strength Differential Effect, Bending Moment

Abstract. The strength differential effect (SDE) (i.e., the tension-compression asymmetry of stress-strain curves), for a ferritic stainless steel sheet was measured using an in-plane compression test. It was found that the in-plane compressive flow stress was 4-7% higher than the uniaxial tensile flow stress in both the rolling and transverse directions. In addition, bending moment-curvature curves were obtained from a pure bending test. These curves were found to be in good agreement with those calculated with SDE taken into account. Thus, the validity of the measured SDE was confirmed by the bending experiment.

Introduction

Stainless steel sheets are used for automotive exhaust system components because of their superior corrosion and heat resistance. Among the various types of stainless steel, ferritic stainless steel, which is less expensive than austenitic stainless steel and has superior thermal fatigue characteristics, has seen increasing use [1]. Automotive parts are often produced by press forming, in which the materials are subjected to tensile and compressive stresses. The strength differential effect (SDE) has been observed in steel sheets [2]-[9]. Kuwahara et al. [10] measured the SDE in austenitic stainless steel sheets used for electronic components and quantitatively clarified its effect on the prediction of springback in bending. Noma et al. [8] improved the prediction accuracy of springback in forming simulations of curved panels by using a material model that takes into account the SDE of a high-strength steel sheet. Yoon et al. [11] implemented the hydrostatic pressure dependency of the distortional plasticity model HAH_{20} [12] using a finite element code to account for the SDE observed in advanced high-strength steel sheets. The implementation was validated by comparing the finite element prediction of the material behavior during U-draw bending and B-pillar forming. However, to the authors' knowledge, no studies have measured the SDE of ferritic stainless steel sheets.

The objective of this study is to measure the SDE of a 1.0-mm-thick Fe-18Cr-3Al ferritic stainless steel sheet. First, uniaxial tensile tests and in-plane compression tests (IPCTs) using an in-plane stress reversal test apparatus [7] are conducted to quantitatively evaluate the magnitude of the SDE. Next, bending moment-curvature ($M-\kappa$) curves are obtained using a pure bending test apparatus. It is found that the experimental $M-\kappa$ curves are consistent with those calculated using the tensile and compressive stress-strain (ss) curves in both the rolling direction (RD) and

transverse direction (TD). Thus, the validity of the measured SDE is confirmed by the bending experiment.

Experimental methods

Test material. The test material used in this study was a 1.0-mm-thick ferritic stainless steel sheet (Fe-18Cr-3Al). The mechanical properties obtained from uniaxial tensile tests are listed in Table 1.

Table 1 Mechanical properties of test material (Fe-18Cr-3Al).

Loading direction	Young's modulus E [GPa]	0.2 % proof stress [MPa]	Tensile strength [MPa]	C* [MPa]	α*	n*	r-value**
RD	195	428	567	960	0.014	0.207	1.12
TD	214	454	587	1003	0.022	0.216	1.78

*Approximated using $\sigma = C(\alpha + \varepsilon^{\mathrm{p}})^n$ at $\varepsilon^{\mathrm{p}} = 0.002$~Maximuim load point
**Measured at an uniaxial nominal strain of 0.1

In-plane compression test. Fig. 1 shows the IPCT apparatus used in this study. This apparatus was first developed by Kuwabara et al. [6], subsequently modified [10], and used in several studies [7-9, 13]. Fig. 1(a) shows an overview of the dies used for applying in-plane compression to a sheet specimen. Fig. 1(b) shows an overview of the test apparatus. A detailed description of the apparatus is given elsewhere [7]. In this study, the blank holding force applied to the specimen was 1% of the 0.2% proof stress (5.7 MPa). The strain was measured using a strain gauge (YFLA-2-1LJC-F, Tokyo Measuring Instruments Laboratory Co. Ltd.). The strain rate was approximately 5×10^{-4} s^{-1} and the testing temperature was room temperature for both tension and compression experiments. Maeda et al. [7] experimentally verified that the effect of frictional force between the upper and lower dies and the specimen on the accuracy of stress measurement can be neglected for the test apparatus shown in Fig. 1. Through in-plane compression tests with a constant gap between the upper and lower dies, Akiyama et al. [14] demonstrated that the blank holding pressure had little effect on the magnitude of compressive flow stress.

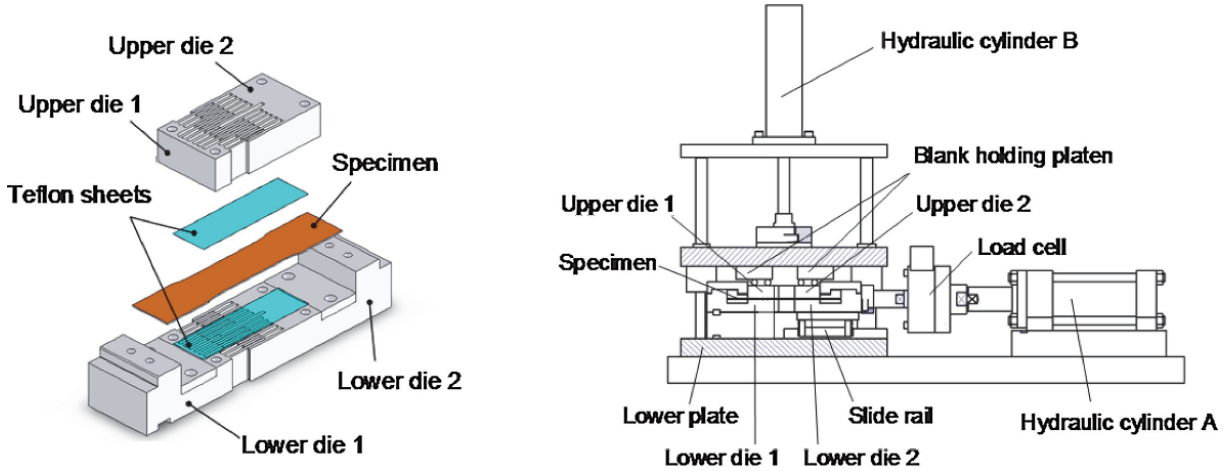

(a) (b)

Fig. 1 IPCT apparatus [7]: (a) upper and lower dies and (b) overview of test apparatus

Fig. 2 shows the geometry of the specimen used in the in-plane compression test. Noma and Kuwabara [13] performed finite element analyses to evaluate the uniformity of the stress

distribution at the gauge section of a specimen subjected to in-plane tension-compression and found that the stress measurement error at the strain gauge location was less than 1%.

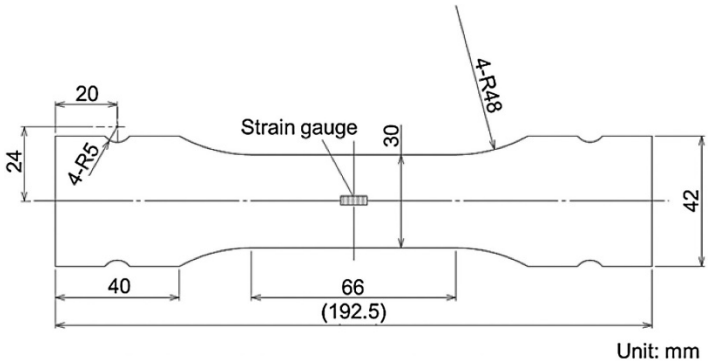

Fig. 2 Geometry of specimen for in-plane tension-compression test

Pure bending test. Pure bending tests were performed to verify the accuracy of the SDE test results. Fig. 3(a) shows an overview of the pure bending test apparatus used in this study. An electric cylinder applies a bending force F to steel wires connected to the bending unit. The magnitude of $2F$ is measured using the load cell. Fig. 3(b) shows the details of the bending unit. Both ends of the specimen are fixed to two fan-shaped blocks, as shown in Fig. 3(c). A steel wire is wound around the block with a circular side, the radius of which is R. Each block has a rotary shaft and rotates around the axis when F is applied via the steel wire. The rotary shafts are connected to the ball bearings bolted to the upper and lower slide guides; therefore, each block can move freely in the horizontal direction during the bending test, preventing the application of a tensile force to the specimen. Thus, a pure bending moment M can be applied to the specimen. M is calculated as

$$M = FR. \tag{1}$$

The curvature κ of the bent specimen is determined from the values of the tensile and compressive bending strains, $\varepsilon_{\mathrm{N}}^{\mathrm{T}}$ and $\varepsilon_{\mathrm{N}}^{\mathrm{C}}$ (< 0), at the convex and concave surfaces of the bent specimen, respectively, as shown in Eq. (2):

$$\kappa \equiv \frac{1}{r_n} = \frac{\left|\varepsilon_{\mathrm{N}}^{\mathrm{C}}\right| + \varepsilon_{\mathrm{N}}^{\mathrm{T}}}{t}, \tag{2}$$

where r_n is the bending radius of the neutral plane at which the bending strain becomes zero (see next section). $\varepsilon_{\mathrm{N}}^{\mathrm{T}}$ and $\varepsilon_{\mathrm{N}}^{\mathrm{C}}$ are measured using high-elongation strain gauges (Kyowa Electronic Instruments Co., KFG-1N120-C1-11) glued to both sides of the specimen, as shown in Fig. 4.

Fig. 4 shows the geometry of the specimen used in the pure bending test. The specimen was fabricated using wire electric discharge machining. The ratio of the width of the gauge section to the sheet thickness was 1.5. Maeda et al. [7] performed a finite element analysis on this specimen geometry and found that the stress state at the gauge section of the bending specimen could be assumed to be uniaxial in both the tensile and compressive sections. This means that M can be directly calculated using the uniaxial tensile and compressive stress-strain (ss) curves. See the next section for details of the calculation procedure for M.

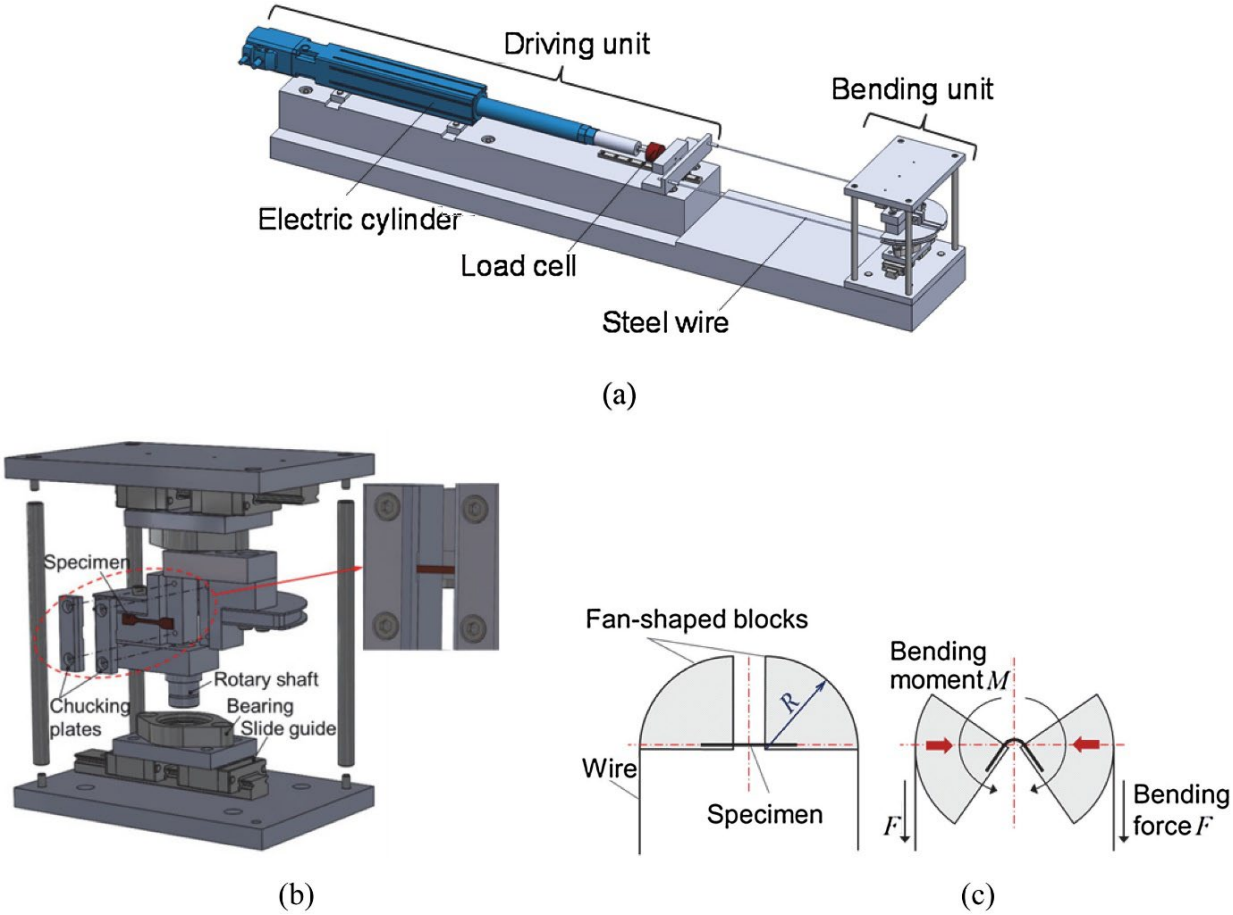

Fig. 3 Experimental apparatus for applying pure bending moment to sheet specimen: (a) overview of test apparatus, (b) overview of bending unit, and (c) pure bending mechanism for bending unit

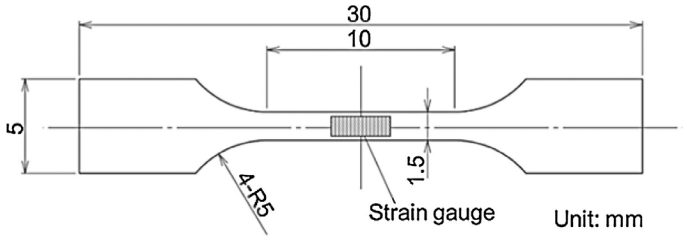

Fig. 4 Geometry of specimen and mounting position of strain gauges for pure bending test

Method for calculating bending moment–curvature curve

To validate the SDE, the $M-\kappa$ curves of samples were calculated and compared with the measurements. In the calculation of an $M-\kappa$ curve, we assumed the following.

(i) The specimen sheet thickness was divided into 100 thin layers of equal thickness. The i-th layer counted from the innermost concave surface of the bent specimen is denoted as layer i. The subscript i is attached to the values related to layer i.

(ii) The x and y axes were taken in the longitudinal and normal (through-thickness) directions of the specimen, respectively. y was taken to be zero on the neutral plane.

(iii) The specimen was subjected to pure bending; the resultant force in the longitudinal direction of the specimen was zero.

(iv) The cross section of the sheet remained planar and normal to the x axis during the bending process.
(v) Each layer in the normal direction of the specimen was subjected to uniaxial tensile or compressive stress, σ_i; σ_i was the only non-zero stress component in the specimen.
(vi) Each layer in the normal direction of the specimen followed the ss curves, as determined by Eq. (3), during the bending process, depending on the magnitude of the bending strain for each layer.

Figs. 5(a) and 5(b) show the measured uniaxial tensile and in-plane compressive ss curves in the RD and TD, respectively. The measured ss curves were approximated using the analytical functions:

$$\sigma = 1000E\varepsilon \text{ for } |\varepsilon| \leq |\varepsilon_{\mathrm{E}}|, \tag{3a}$$

$$\sigma = 1000E\varepsilon_{\mathrm{E}} + \frac{\sigma_{\mathrm{Mid}} - 1000E\varepsilon_{\mathrm{E}}}{\varepsilon_{\mathrm{Mid}} - \varepsilon_{\mathrm{E}}}(\varepsilon - \varepsilon_{\mathrm{E}}) \text{ for } |\varepsilon_{\mathrm{E}}| < |\varepsilon| < |\varepsilon_{\mathrm{Mid}}|, \tag{3b}$$

$$\sigma = \frac{\sigma_{\mathrm{Mid}} - \{a - b\exp(-c\varepsilon)\}}{\varepsilon_{\mathrm{Mid}} - \varepsilon_{\mathrm{E}}}(\varepsilon - \varepsilon_{\mathrm{Mid}}) + \sigma_{\mathrm{Mid}} \text{ for } |\varepsilon_{\mathrm{Mid}}| < |\varepsilon| < |\varepsilon_{\mathrm{P}}|, \tag{3c}$$

$$\sigma = \pm\{a - b\exp(-c\varepsilon)\} \text{ for } |\varepsilon_{\mathrm{P}}| \leq |\varepsilon|, \tag{3d}$$

where ε_{E} is the upper limit of the elastic strain range and ε_{P} is the lower limit of the elastic-plastic strain range, for which the ss curve was approximated using Voce's hardening law, $\sigma = a - b\exp(-c\varepsilon)$. The ss curves for $|\varepsilon_{\mathrm{E}}| < |\varepsilon| < |\varepsilon_{\mathrm{P}}|$ sections were approximated by two straight lines, namely one for $\varepsilon_{\mathrm{E}} \leq \varepsilon < \varepsilon_{\mathrm{Mid}}$ and one for $\varepsilon_{\mathrm{Mid}} \leq \varepsilon < \varepsilon_{\mathrm{P}}$. The plus and minus signs in Eq. (3d) are for tension ($\varepsilon \geq 0$) and compression ($\varepsilon < 0$), respectively. Table 2 summarizes the parameter values used in Eq. (3).

When the curvature of the neutral plane is κ, the logarithmic longitudinal strain, ε, of a layer at a coordinate y is given by

$$\varepsilon = \ln(1 + \kappa y). \tag{4}$$

The force balance equation is

$$\sum_{j=1}^{100} \sigma_j^{\mathrm{T}} \cdot w_j \cdot \Delta y_j + \sum_{k=1}^{100} \sigma_k^{\mathrm{C}} \cdot w_k \cdot \Delta y_k = 0, \tag{5}$$

where w_i and Δy_i are the width and thickness of the i-th layer, respectively. The position of the neutral plane, at which $y = 0$, was determined to satisfy Eq. (5).

The bending moment M can be calculated as

$$M = \sum_{j=1}^{100} \sigma_j^{\mathrm{T}} \cdot y_j \cdot w_j \cdot \Delta y_j + \sum_{k=1}^{100} \sigma_k^{\mathrm{C}} \cdot y_k \cdot w_k \cdot \Delta y_k . \tag{6}$$

Table 2 Summary of parameter values used in Eq. (3).

Loding direction	Loading mode	E [GPa]	r-value	a* [MPa]	b* [MPa]	c*	ε_E	ε_P	ε_{mid}	σ_{mid} [MPa]
RD	Tension	195	1.12	753.0	339.3	8.969	0.0017	0.0040	0.0026	405
	Compression	186	1.15	808.9	379.6	9.677	0.0016	0.0035	0.0025	400
TD	Tension	214	1.78	755.2	315.9	9.529	0.0018	0.0030	0.0022	426
	Compression	222	1.93	854.2	397.2	8.745	0.0017	0.0025	0.0022	446

*Approximated using $\sigma = a - b\exp(-c\varepsilon^{\mathrm{p}})$

Experimental results and discussion

SDE in uniaxial stress states. Figs. 5(a) and 5(b) compare the uniaxial tensile true stress-logarithmic plastic strain curves, $\sigma^{\mathrm{T}} - \varepsilon^{\mathrm{p}}$, with the compressive ones, $|\sigma^{\mathrm{C}}| - |\varepsilon^{\mathrm{p}}|$, measured using the IPCT for the RD and TD, respectively. Each curve is the average of two measurements. The flow stresses are higher in compression than in tension in both directions. Therefore, the SDE was clearly observed. To quantitatively evaluate the magnitude of the SDE in the uniaxial stress state, the rate of increase of the flow stress, β_{SDE}, was defined as

$$\beta_{\mathrm{SDE}} = 2\frac{|\sigma^{\mathrm{C}}| - \sigma^{\mathrm{T}}}{|\sigma^{\mathrm{C}}| + \sigma^{\mathrm{T}}}, \tag{8}$$

where σ^{T} and $|\sigma^{\mathrm{C}}|$ are the measured values of the tensile and compressive flow stresses, respectively, at a given plastic work per unit volume, w^{p}. Fig. 6 shows the variation of β_{SDE} with w^{p} for the RD and TD. It was found that $0.001 < \beta_{\mathrm{SDE}} < 0.064$ for the RD and $0.041 < \beta_{\mathrm{SDE}} < 0.073$ for the TD; therefore, the test sample clearly exhibited the SDE.

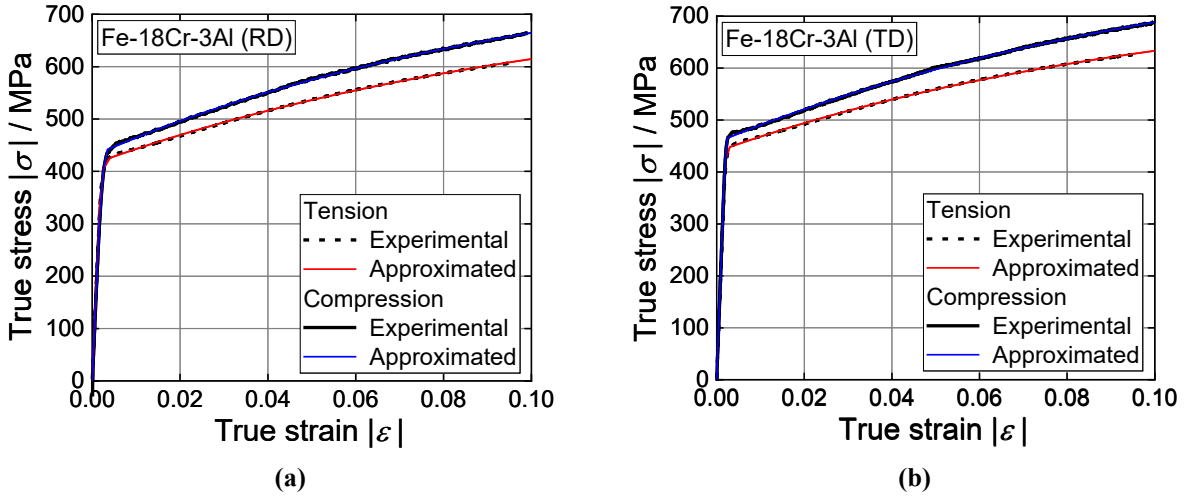

Fig. 5 Comparison of true stress-logarithmic strain curves for tension and compression in (a) RD and (b) TD

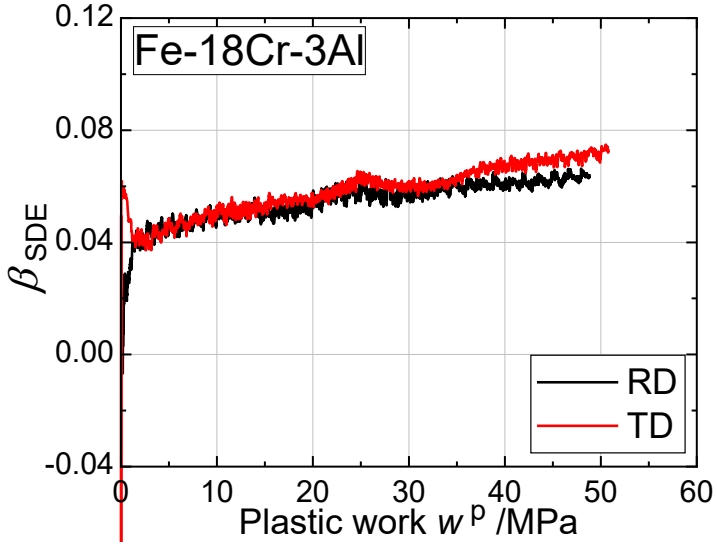

Fig. 6 Change in β_{SDE} with plastic work per unit volume

The magnitude of β_{SDE} is 0.05-0.06 for a 980 MPa dual phase steel sheet [7] and 0.02-0.10 for a cold rolled steel sheet [9]. Therefore, the magnitude of β_{SDE} of the test sample used in this study (Fig. 6) is the same level of the steel sheets.

$M-\kappa$ curve. Fig. 7(a) and 7(b) compare the experimental and calculated $M-\kappa$ curves for the RD and TD, respectively. The three experimental curves, 1, 2 and 3, are consistent with each other in both directions, confirming the reproducibility of the experimental data. The red curves are the $M-\kappa$ curves calculated without considering the SDE; it was assumed that both the tensile and compressive ss curves follow the tensile ss curve approximated by Voce's hardening law shown in Eq. (3). The blue curves are the $M-\kappa$ curves calculated considering the SDE. The blue curves are higher than the red ones for a range of $\kappa \geq 10$ m^{-1} in both directions. This was expected, as the flow stresses were higher in compression than in tension, as shown in Fig. 5. Furthermore, in both directions, the $M-\kappa$ curves calculated considering the SDE reproduced the experimental ones more accurately than did those calculated without considering the SDE. Thus, the SDE shown in Figs. 5 and 6 is validated by the pure bending experiment.

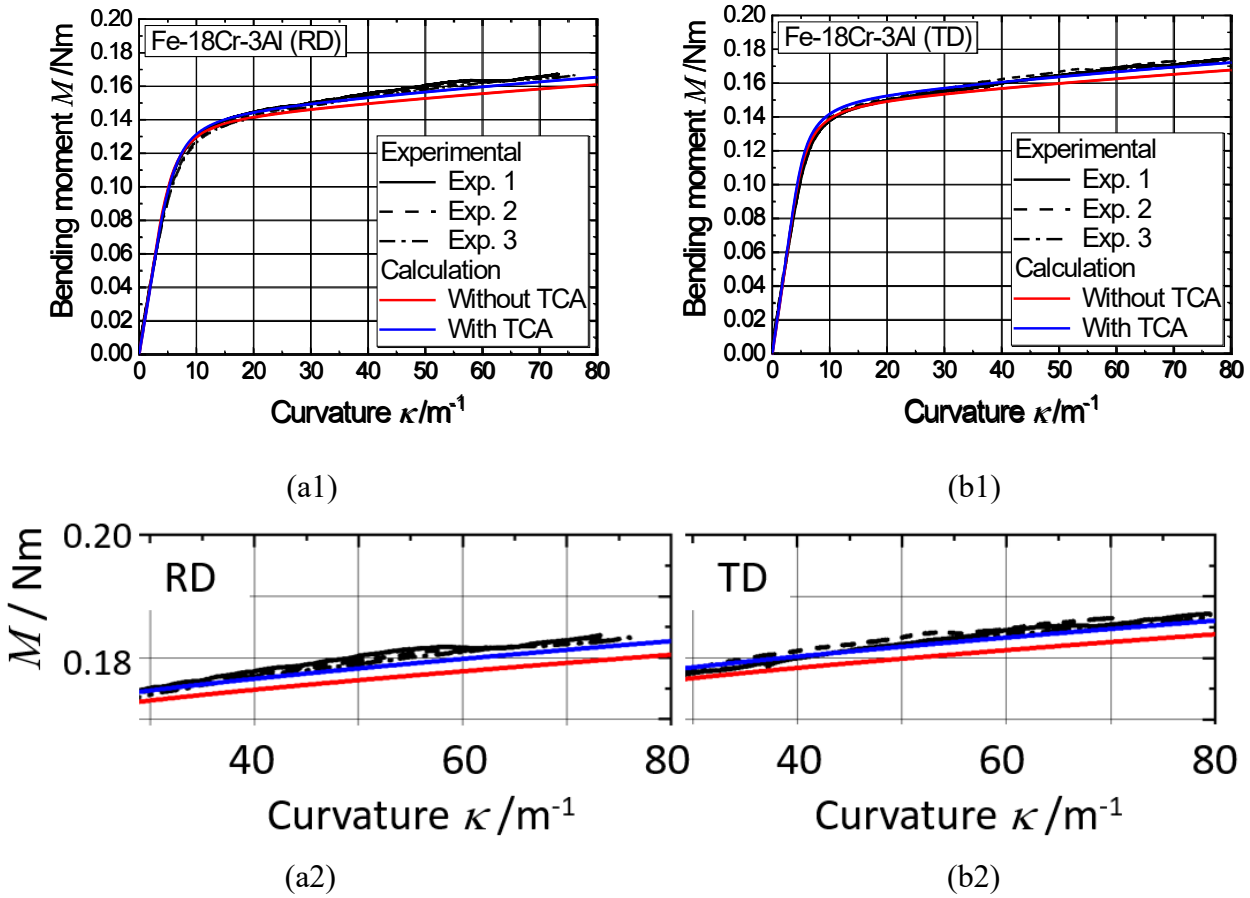

Fig. 7 Comparison of measured $M-\kappa$ curves with calculated ones in (a1) and (a2) RD and (b1) and (b2) TD. (a2) and (b2) are the enlarged figures of (a1) and (b1), respectively.

Conclusions

Uniaxial tensile and in-plane compression tests were performed on a ferritic stainless steel sheet to measure the SDE. A pure bending test was performed to experimentally verify the SDE. The experimental findings obtained in this study can be summarized as follows.

(1) The SDE was observed for the test samples ($0.001<\beta_{SDE}<0.064$ for the RD and $0.041<\beta_{SDE}<0.073$ for the TD).

(2) The experimental $M-\kappa$ curves were consistent with those calculated using the tensile and compressive ss curves obtained from the tension and compression experiments in both the RD and TD. Thus, the validity of the measured SDE was confirmed by the bending experiment.

References

[1] J. Hamada, A. Hayashi, N. Kanno, T. Komori, H. Ito, N. Fukuda, Y. Inoue, Development of Heat-resistant Ferritic Stainless Steels "NSSC429NF" and "NSSC448EM" Utilized Dynamic Precipitation Hardening for Automotive Exhaust Systems, Materia Japan 56 (2017) 33-35. (in Japanese) https://doi.org/10.2320/materia.56.33

[2] W.A. Spitzig, R.J. Sober, O. Richmond, Pressure dependence of yielding and associated volume expansion in tempered martensite, Acta Metall. 23 (1975), 885-893. https://doi.org/10.1016/0001-6160(75)90205-9

[3] W.A. Spitzig, R.J. Sober, O. Richmond, O., The effect of hydrostatic pressure on the deformation behavior of maraging and HY-80 steels and its implication for plasticity, Met. Trans. 7A (1976) 1703-1710. https://doi.org/10.1007/BF02817888

[4] O. Richmond, W.A. Spitzig, Pressure dependence and dilatancy of plastic flow, IUTAM Conference, Theoretical and Applied Mechanics, Proc. 15th International Congress of Theoretical and Applied Mechanics. North-Holland Publishers, Amsterdam, 1980, pp. 377–386.

[5] W.A. Spitzig, O. Richmond, The effect of pressure on the flow stress of metals, Acta Metall. 32 (1984) 457-463. https://doi.org/10.1016/0001-6160(84)90119-6

[6] T. Kuwabara, Y. Morita, Y. Miyashita, S. Takahashi, Elastic-Plastic Behavior of Sheet Metal Subjected to In-Plane Reverse Loading, in S. Tanimura, A.S. Khan (Eds.), Proc. Plasticity '95, The fifth international symposium on plasticity and its current applications, Gordon and Breach Publishers, 1995, pp.841-844,.

[7] T. Maeda, N. Noma, T. Kuwabara, F. Barlat, Y.P. Korkolis, Measurement of the strength differential effect of DP980 steel sheet and experimental validation using pure bending test, J. Mater. Process. Technol. 256 (2018) 247-253. https://doi.org/10.1016/j.jmatprotec.2018.02.009

[8] N. Noma, K. Hashimoto, T. Maeda, T. Kuwabara, Enhancement of Accuracy of Springback Simulation Using the Material Model Considering the Strength Differential Effect, J. JSTP 61 (2020) 20-25. (in Japanese). https://doi.org/10.9773/sosei.61.20

[9] T. Kuwabara, R. Tachibana, Y. Takada, T. Koizumi, S. Coppieters, F. Barlat, Effect of hydrostatic stress on the strength differential effect in low-carbon steel sheet, Int. J. Material Forming 15 (2022) 13. https://doi.org/10.1007/s12289-022-01650-2

[10] T. Kuwabara, R. Saito, T. Hirano, N. Oohashi, Tension–Compression Asymmetry of SUS304 Stainless Sheet for Electronic Parts and Its Effects on Bending and Springback Behavior, Tetsu-to-Hagané 95 (2009) 732-739. (in Japanese). https://doi.org/10.2355/tetsutohagane.95.732

[11] S.Y. Yoon, F. Barlat, S.Y. Lee, J.H. Kim, M.S. Wi, D.J. Kim, Finite element implementation of hydrostatic pressure-sensitive plasticity and its application to distortional hardening model and sheet metal forming simulations, J. Mater. Processing Technol. 302 (2022) 117494. https://doi.org/10.1016/j.jmatprotec.2022.117494

[12] F. Barlat, S.Y. Yoon, S.Y. Lee, M.S. Wi, J.H. Kim, Distortional plasticity framework with application to advanced high strength steel, Int. J. Solids Struct. 202 (2020) 947-962.

https://doi.org/10.1016/j.ijsolstr.2020.05.014

[13] N. Noma, T. Kuwabara, Specimen Geometry Optimization for In-plane Reverse Loading Test of Sheet Metal and Experimental Validation, J. JSTP 53 (2012) 574-579. (in Japanese). https://doi.org/10.9773/sosei.53.574

[14] K. Akiyama, R. Tachibana, T. Sakurai, T. Kuwabara: submitted to J. Materials Processing Technology (2024).